BRAIN COMMUNICATIONS

# Progression of regional cortical cholinergic denervation in Parkinson's disease

Nicolaas I. Bohnen,[1,2,3,4,5] Stiven Roytman,[1] Prabesh Kanel,[1,4,5] Martijn L. T. M. Müller,[1,6] Peter J. H. Scott,[1] Kirk A. Frey,[1,4] Roger L. Albin[2,3,4,5] and Robert A. Koeppe[1,4]

Cortical cholinergic deficits contribute to cognitive decline and other deficits in Parkinson's disease. Cross-sectional imaging studies suggest a stereotyped pattern of posterior-to-anterior cortical cholinergic denervation accompanying disease progression in Parkinson's disease. We used serial acetylcholinesterase PET ligand imaging to characterize the trajectory of regional cholinergic synapse deficits in Parkinson's disease, testing the hypothesis of posterior-to-anterior progression of cortical cholinergic deficits. The 16 Parkinson's disease subjects (4 females/12 males; mean age: 64.4 ± 6.7 years; disease duration: 5.5 ± 4.2 years; Hoehn & Yahr stage: 2.3 ± 0.6 at entry) completed serial $^{11}$C-methyl-4-piperidinyl propionate acetylcholinesterase PET scans over a 4–8 year period (median 5 years). Three-dimensional stereotactic cortical surface projections and volume-of-interest analyses were performed. Cholinergic synapse integrity was assessed by the magnitude, $k_3$, of acetylcholinesterase hydrolysis of $^{11}$C-methyl-4-piperidinyl propionate. Based on normative data, we generated *Z*-score maps for both the $k_3$ and the $k_1$ parameters, the latter as a proxy for regional cerebral blood flow. Compared with control subjects, baseline scans showed predominantly posterior cortical $k_3$ deficits in Parkinson's disease subjects. Interval change analyses showed evidence of posterior-to-anterior progression of cholinergic cortical deficits in the posterior cortices. In frontal cortices, an opposite gradient of anterior-to-posterior progression of cholinergic deficits was found. The topography of $k_3$ changes exhibited regionally specific disconnection from $k_1$ changes. Interval-change analysis based on $k_3/k_1$ ratio images ($k_3$ adjustment for regional cerebral blood flow changes) showed interval reductions (up to 20%) in ventral frontal, anterior cingulate and Brodmann area 6 cortices. In contrast, interval $k_3$ reductions in the posterior cortices, especially Brodmann areas 17–19, were largely proportional to $k_1$ changes. Our results partially support the hypothesis of progressive posterior-to-cortical cholinergic denervation in Parkinson's disease. This pattern appears characteristic of posterior cortices. In frontal cortices, an opposite pattern of anterior-to-posterior progression of cholinergic deficits was found. The progressive decline of posterior cortical acetylcholinesterase activity was largely proportional to declining regional cerebral blood flow, suggesting that posterior cortical cholinergic synapse deficits are part of a generalized loss of synapses. The disproportionate decline in regional frontal cortical acetylcholinesterase activity relative to regional cerebral blood flow suggests preferential loss or dysregulation of cholinergic synapses in these regions. Our observations suggest that cortical cholinergic synapse vulnerability in Parkinson's disease is mediated by both diffuse processes affecting cortical synapses and processes specific to subpopulations of cortical cholinergic afferents.

1 Department of Radiology, University of Michigan, Ann Arbor, MI 48109, USA
2 Department of Neurology, University of Michigan, Ann Arbor, MI 48109, USA
3 Neurology Service and GRECC, VA Ann Arbor Healthcare System, Ann Arbor, MI 48105, USA
4 Morris K. Udall Center of Excellence for Parkinson's Disease Research, University of Michigan, Ann Arbor, MI 48109, USA
5 Parkinson's Foundation Research Center of Excellence, University of Michigan, Ann Arbor, MI 48109, USA
6 Parkinson Consortium, Critical Path Institute, Tucson, AZ 85718, USA

Correspondence to: Nicolaas I. Bohnen, MD, PhD
Functional Neuroimaging, Cognitive and Mobility Laboratory
Department of Radiology and Department of Neurology
University of Michigan, 24 Frank Lloyd Wright Drive
Box 362, Ann Arbor, MI 48105-9755, USA
E-mail: nbohnen@umich.edu

Received May 23, 2022. Revised September 13, 2022. Accepted December 01, 2022. Advance access publication December 2, 2022
Published by Oxford University Press on behalf of the Guarantors of Brain 2022.

**Keywords:** acetylcholinesterase; progressive cholinergic denervation; Parkinson's disease; PET

**Abbreviations:** BA = Brodmann area; PMP = methyl-4-piperidinyl propionate

**Graphical Abstract**

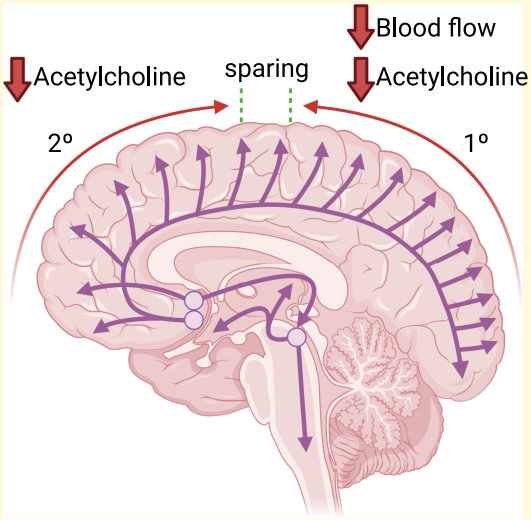


# Introduction

Parkinson's disease is recognized as a multi-system neurodegenerative disorder with variations in clinical features that, in part, are attributable to deficits of multiple neurotransmitter systems.[1] In addition to the defining degeneration of dopaminergic pathways, there is considerable evidence for clinically impactful alterations of cholinergic pathways in Parkinson's disease.[2-4] There are two major brain cholinergic projection systems. The first arises from the basal forebrain complex, providing cholinergic innervation to the cortical mantle and related structures such as the hippocampal formation and the amygdala.[5, 6] The second arises from the mesopontine cholinergic neurons, the pedunculopontine–laterodorsal tegmental complex, providing cholinergic inputs to the thalamus, basal ganglia, superior colliculus, other brainstem nuclei and the spinal cord.[7-9] Both of these systems degenerate in Parkinson's disease, contributing to important treatment refractory features of Parkinson's disease, including cognitive decline, postural instability and gait deficits.[3, 4]

Cortical cholinergic deficits may play a particularly important role in cognitive decline in Parkinson's disease. Early post-mortem studies indicated that basal forebrain cholinergic system degeneration is associated with dementia in Parkinson's disease.[10-12] The development of molecular imaging methods allowing *in vivo* assessments of regional brain cholinergic synapse-terminal density verified the association between cortical cholinergic deficits and Parkinson's disease dementia. The initially applied methods were acetylcholinesterase PET and vesicular acetylcholine transporter single-photon emission tomography. Application of these methods showed that Parkinson's disease dementia is associated with more severe and widespread cholinergic denervation compared with Parkinson's disease without dementia.[13-16] Acetylcholinesterase PET imaging assesses cholinergic synapse integrity, with cortical uptake reflecting largely basal forebrain integrity and thalamic uptake principally reflecting mesopontine cholinergic neuron integrity. A comparison of Parkinson's disease and Parkinson's disease dementia subjects with acetylcholinesterase PET and vesicular acetylcholine transporter single-photon emission computerized tomography showed more prominent posterior cortical cholinergic losses in Parkinson's disease dementia. These results contributed to the dual syndrome model of Kehagia *et al.*[17] which posits initial cognitive impairments secondary to frontostriatal system dysfunction secondary to nigrostriatal dopaminergic deficits with subsequent multi-domain cognitive deficits secondary-to-posterior cortical dysfunctions, driven at least partly by cholinergic denervation. These cross-sectional imaging results also suggested a posterior-to-anterior progression of cortical cholinergic denervation as Parkinson's disease progresses to Parkinson's disease dementia.[18, 19] The connectional anatomy of basal forebrain cholinergic projections indicates that most posterior cortical regions are innervated by the longest basal forebrain efferents.[20-22] Basal forebrain cholinergic corticopetal axons have luxuriant terminal arbours, which are probably particularly extensive in the human cortex.[23] A posterior-to-anterior progression of cortical cholinergic denervation is consistent with the hypothesized concept that cholinergic projection system vulnerability is a function of the stresses of supporting abundant terminals at the end of long, poorly myelinated axons.[24] Disruption in anterograde transport at any point along the length of the axon would prevent the delivery of proteins synthesized at the soma to the synaptic terminal, depriving it of the materials necessary for the maintenance and plasticity

of the presynaptic membrane. According to this hypothesis, terminals at the end of the longest cholinergic axons that innervate the posterior cortices would have the greatest vulnerability surface, making them most susceptible to loss of cholinergic input. More prominent cortical cholinergic losses observed in cross-sectional *in vivo* imaging studies have been explained using this argument.[18, 19] An alternative hypothesis for the vulnerability of these neurons to age-related neurodegeneration may be their reliance on retrograde axonal transport for neurotrophic support.[25] The basal forebrain cholinergic corticopetal projection system was traditionally conceived as a diffuse, nonspecific neuromodulatory system.[5] Recent studies, however, indicate that the basal forebrain cholinergic corticopetal system is organized as clusters of neurons innervating multiple cortical regions, with the governing rule that interconnected cortical fields receive cholinergic innervation from the same basal forebrain neuron cluster.[26, 27] Functional studies suggest that basal forebrain clusters function independently and that basal forebrain cholinergic neuron signalling has phasic and stimulus-specific components.[28, 29] The emerging data indicating anatomic and functional heterogeneity of basal forebrain corticopetal cholinergic projections suggests an alternative to the pathogenic model of length-dependent degeneration—relatively selective degeneration of clusters of basal forebrain cholinergic corticopetal projections.

The cross-sectional design of prior cholinergic synapse imaging studies largely precludes differentiation of these two hypotheses regarding the pattern of cortical cholinergic synapse deficits in Parkinson's disease. The length-dependent model predicts a strictly posterior-to-anterior gradient. Relatively early loss of cortical cholinergic synapses in more anterior regions would be more consistent with a cluster-based model of degeneration. To the best of our knowledge, there are no prior longitudinal cholinergic synapse-terminal PET or single-photon emission computerized tomography imaging studies examining regional cortical interval changes in Parkinson's disease. A prior longitudinal acetylcholinesterase PET study in seven patients with Alzheimer's disease reported only global cortical losses of about $3.8 \pm 2.5\%$ per year over a 2-year period but did not comment on regional cortical interval changes.[30] We set out to examine the evolution of the topography of cortical cholinergic denervation in a longitudinal acetylcholinesterase PET imaging analysis of Parkinson's disease subjects, relative to a normal control comparison group and over a 4–8-year period. We hypothesized that the evolution of acetylcholinesterase deficits would follow a posterior-to-anterior progression.

# Materials and methods

## Subjects

The 16 patients with Parkinson's disease (4 females/12 males; mean age: $64.4 \pm 6.7$ years, duration of the disease: $5.5 \pm 4.2$ years and Hoehn & Yahr stage: $2.3 \pm 0.6$ at entry) completed serial $^{11}$C-methyl-4-piperidinyl propionate [($^{11}$C)-PMP] acetylcholinesterase PET scans over a 4–8-year (median: 5 years) in a historical cohort study. The study population was based on a convenience sample of study participants enrolled in various [$^{11}$C]-PMP PET studies at our centre during the period 2006–15 and having a repeat PET scan available at least 4 years after the baseline scan. Parkinson's disease subjects met the UK Parkinson's Disease Society Brain Bank clinical diagnostic criteria.[31] No subjects were treated with anti-cholinergic or cholinesterase inhibitor drugs. The study was approved, and the study procedures were followed in accordance with the ethical standards of the Institutional Review Boards of the University of Michigan and Veterans Affairs Ann Arbor Health System for studies involving human subjects. Written informed consent was obtained from all subjects. Motor and non-motor clinical correlates of acetylcholinesterase PET in this population were described previously.[32]

## Imaging techniques

All subjects underwent brain magnetic resonance imaging and [$^{11}$C]-PMP acetylcholinesterase PET imaging. Magnetic resonance imaging was performed on a 3T Philips Achieva system (Philips, Best, The Netherlands) utilizing an eight-channel head coil and the 'ISOVOX' exam card protocol, primarily designed to yield isotropic spatial resolution. A standard $T_1$-weighted series of a 3D inversion recovery-prepared turbo-field-echo was performed in the sagittal plane using repetition time/time to echo/inversion time = 9.8/4.6/1041 ms; turbo factor = 200; single average; field-of-view = $240 \times 200 \times 160$ mm; acquired matrix = $240 \times 200$. One hundred and sixty slices were reconstructed to 1 mm isotropic resolution. This sequence maximizes contrast among grey matter, white matter and cerebrospinal fluid and provides high-resolution delineation of cortical and subcortical structures.

[$^{11}$C]-PMP PET imaging was performed in 3D imaging mode using an ECAT HR + tomograph (Siemens Molecular Imaging, Inc., Knoxville, TN), which acquired 63 trans-axial slices (slice thickness: 2.4 mm; intrinsic in-plane resolution: 4.1 mm full-width at half maximum over a 15.2 cm axial field-of-view). A NeuroShield (Scanwell Systems, Montreal, Canada) head-holder/shielding unit was applied to the patient bed to reduce the contribution of detected photon events originating from the body outside the scanner field-of-view.[33] Prior to the PMP injections, a 5 min transmission scan was acquired using rotating $^{68}$Ge rods for attenuation correction of emission data using the standard vendor-supplied segmentation and re-projection routines.

[$^{11}$C]-PMP was prepared in high radiochemical purity (>95%) by N-[$^{11}$C]-methylation of piperidine-4-yl propionate using a previously described method.[34] Dynamic PET scanning was performed for 70–80 min following a bolus injection of 15 mild cognitive impairment (MCI) [$^{11}$C]-PMP.[35]

## Imaging and statistical analysis

All image frames were spatially coregistered within subjects with a rigid-body transformation to reduce the effects of

subject motion during the imaging session.[36] Interactive data language image analysis software (Research Systems, Inc., Boulder, CO) was used to manually trace volumes-of-interest on MRI images to include the thalamus, caudate nucleus and putamen of each hemisphere. Acetylcholinesterase [$^{11}$C]-PMP hydrolysis rates ($k_3$) were estimated using the striatal volume-of-interest (defined by manual tracing on the magnetic resonance imaging scan of the putamen and caudate nucleus) as the tissue reference for the integral of the precursor delivery reference tissue-based linear least squares analysis.[37, 38] The quantitative parametric images were transformed into the bicommissural stereotactic coordinate system using a method described previously.[39, 40] Differences in individual brain sizes were removed by linear scaling and regional anatomic differences were minimized by a non-linear warping technique[40] (mean age: 66.7 ± 7.3 years). Cortical grey matter activities were extracted to a standard set of voxels covering the entire brain surface using 3D stereotactic surface projections (3D-SSPs).[41] This cortical data extraction technique compensates for small anatomical differences in grey matter structures (such as variable depth of gyri) across subjects and minimizes partial volume artefacts and the effects of atrophy. Voxel-based *Z*-score cortical maps were generated based on normative data from 61 normal older controls (mean age: 66.7 ± 7.3 years) for Parkinson's disease versus control group comparison and for within-Parkinson's disease group longitudinal analysis.

A limitation of [$^{11}$C]-PMP PET is that it does not allow accurate assessment of the high acetylcholinesterase activity levels within the striatum and cerebellar cortex but has reasonable estimation in the thalamus and limbic structures (amygdala, hippocampal formation, insular cortex).[38] Striatum and cerebellum were excluded from analysis, with thalamus and limbic structures analysed separately with an exploratory *post hoc* linear mixed model.

We complemented this analysis by comparing bilaterally averaged volume-of-interest-based percentage differences between Visits 1 and 2 using a Brodmann area (BA) atlas.[42]Per cent change in hydrolysis rates ($\%\Delta k_3$) and a regional cerebral blood flow proxy ($\%\Delta k_1$) was mapped onto BA volume-of-interests and visualized on a high-resolution cortical surface mesh. The ratio of $\%\Delta k_3$ over $\%\Delta k_1$ was visualized to highlight changes in acetylcholinesterase hydrolysis rates relative to changes in regional blood flow across volume-of-interests. As regional cerebral blood flow is proportional to regional synaptic density, the $\%\Delta k_3/\%\Delta k_1$ ratio normalizes cholinergic synapse changes to diffuse changes in cortical synaptic density. As cortical cholinergic synapses are only a small fraction of cortical synapses, cortical cholinergic synaptic deficits, by themselves, would not be expected to markedly influence total regional synaptic density. The volume-of-interest-based cortical surface plots were generated using *Nilearn*, an open-source neuroimaging Python module based upon many machine learning algorithms provided by Scikit learn.[43]

Performing statistical inference on all the regions would have been infeasible since the need to control for Type I statistical error would lead to overcorrection with this many model comparisons and consequently inflate our Type II statistical error. Since we had no specific a-priori hypothesis about which regions were most likely to yield an effect, we used a pre-inference outcome variable selection approach to reduce Type II statistical error. A volume-of-interest-based BA analysis was performed on a subset of regions with the highest $\%\Delta k_3/\%\Delta k_1$ ratio values, determined heuristically using an elbow plot since we believed that regions with the highest normalized cholinergic synapse change were most likely to yield an effect in a model that accounts for changes in cerebral blood flow. For each region in this subset of regions, a pair of random intercept mixed linear models predicting scaled and centred hydrolysis rates ($k_3$) was estimated. The confounder model served as a null hypothesis and contained only a random intercept for each participant and a fixed effect of scaled and centred proxy flow ($k_1$). The visit model served as an alternate hypothesis and incorporated a fixed effect of binary-coded visits (baseline versus the last visit) in addition to confounding model predictors. The goodness of fit was compared between these two models using a likelihood ratio test. The set of resulting *P*-values was corrected for family-wise error rate using Holm's method.[44] A significant predictor effect of $k_3$ independent of $k_1$ and individual differences in baseline $k_3$ for any region was present when the comparison between the blood flow confounder and visit model yielded a corrected $P$ value $<0.05$. A separate *post hoc* analysis of cholinergic denervation was conducted in four subcortical–limbic structures not assessed by the cortical 3D-SSP analysis (amygdala, insula, thalamus and hippocampus) using a similar statistical procedure as described above. Volume-of-interest-based statistical analyses were conducted using *Statsmodels*, an open-source Python module.[45]

To elucidate the effect of longitudinal cholinergic system changes on clinical manifestations of Parkinson's disease, a series of *post hoc* linear mixed models were estimated. Given prior literature that showed more robust posterior, rather than anterior, cerebral cholinergic losses related to cognitive function in Parkinson's disease, the regressand in all the models was the occipital–parietal $k_3$ cortical hydrolysis rate, which was calculated by taking the average of $k_3$ from BA2, 5, 7, 17, 18, 19, 23, 39, 40, 43 and 51. Examined clinical variables included the presence of visual and auditory hallucinations, MCI, executive function and the presence of rapid eye movement sleep behaviour disorder (RBD) at baseline. Executive function was operationalized as the time in seconds to complete the Delis–Kaplan Executive Function System Stroop III, which is the classic Stroop cognitive interference condition and Stroop IV, a modified version of the Stroop test that includes a rule-switching component.[46] MCI was operationalized as a score below a cut-off of 26 on the Mini-Mental State Examination. All variables included in the analysis were transformed to *Z*-scores to yield standardized $\beta$ coefficients in the resulting mixed linear models.

For each clinical regressor, four hierarchical mixed linear models were fitted: a random intercept model, a visit model, an independent effect model and a visit by clinical regressor interaction model. The random intercept model included only a random intercept for each participant to account for baseline differences in occipital–parietal $k_3$. The visit model added a fixed effect of visit on occipital–parietal $k_3$. The independent effect

model added a fixed effect of a clinical regressor on top of the visit model. Finally, the interaction model added an interaction between the visit and the clinical regressor. The Akaike information criterion (AIC) was computed for all four models and the AIC minimizing model was selected for this exploratory analysis.

# Results

## Serial acetylcholinesterase $k_3$ (hydrolysis rates) in the Parkinson's disease group at baseline ($t_1$), second ($t_2$) and third ($t_3$) follow-up imaging visits

Figure 1 displays 3D-SSP images representing absolute acetylcholinesterase $k_3$ in the Parkinson's disease group at baseline and follow-up visits. Difficult to quantify high hydrolysis rate regions, including the cerebellum and striatum, are whited-out. Baseline images show lower $k_3$ in the lateral posterior and inferior temporal, superior parietal and occipital association cortices. There is a relative sparing of primary visual cortices. Higher tracer retention is seen in the primary sensorimotor and precentral cortices, with lower $k_3$ in prefrontal areas. Subsequent changes include more severe posterior cortical deficits and a mid-prefrontal progression of deficits. The latter appears to progress in an anterior-to-posterior (both superior and orbitofrontal directions) pattern of progression. There is the preservation of primary and secondary sensorimotor cortex tracer retention.

## Serial $k_3$ *Z*-score maps over three time points in Parkinson's disease compared with normal older control persons

Figure 2 represents 3D-SSP *Z*-score image analysis (comparison with normative control data). *Z*-score analysis confirms the analysis of absolute $k_3$ changes. At baseline, pronounced reductions (*Z*-scores $< -2$) were found in occipital association cortices, posterolateral and inferior temporal regions, precuneus, posterior cingulum and to a lesser degree, in mesofrontal regions of Parkinson's disease subjects. Progression of deficits was found in posterior cortical and frontal cortical regions, with evidence of a posterior cortical posterior-to-anterior pattern of progression and an anterior cortical anterior-to-posterior pattern of progression.

## *Post hoc* analysis of dissociation of acetylcholinesterase $k_3$ from $k_1$ regional cerebral blood flow proxy changes at baseline

As cortical cholinergic deficits may, in part, reflect diffuse changes in regional synaptic density, we performed a *post hoc* analysis comparing the relative cortical topography of acetylcholinesterase $k_3$ versus $k_1$ regional cerebral blood flow proxy changes in Parkinson's disease subjects at baseline. *Z*-scores based on comparison with normative data are presented in Fig. 3. Relative comparison of $Z(k_3)$ with $Z(k_1)$ scores show topographic dissociation between cortical cholinergic deficits described above compared with more prominent $k_1$ regional cerebral blood flow proxy reductions, particularly in the superior and posterior parietal cortices and anterior and inferior prefrontal cortices with opposite findings of relatively more prominent $k_3$ reductions in the primary sensorimotor strip (Fig. 3).

## Brodmann area volume-of-interest-based percentage difference between Visits 1 and 2

Based on the previously described heuristic elbow plot approach, seven cortical Brodmann areas were chosen for the volume-of-interest-based percentage difference analysis and subsequent mixed linear models (Table 1). Among them,

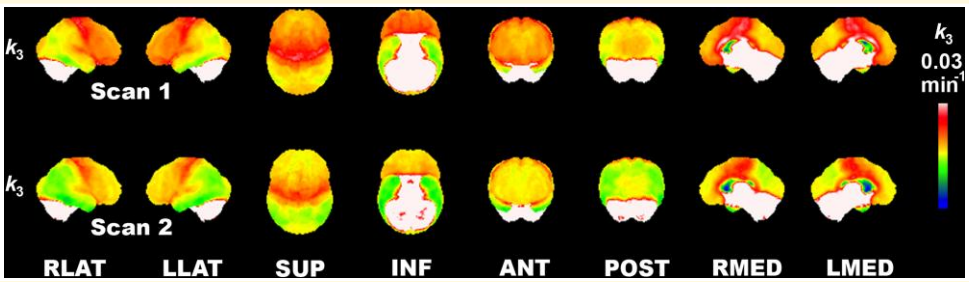


**Figure 1 Longitudinal regional cortical acetylcholinesterase hydrolysis reduction in Parkinson's disease.** 3D-SSP images showing absolute acetylcholinesterase $k_3$ hydrolysis in the Parkinson's disease group at baseline (Scan 1) and follow-up (Scan 2). High-intensity-binding areas, including the cerebellum and striatum, are whited-out as these cannot be estimated reliably. Findings show a lower hydrolysis rate in the lateral posterior and inferior temporal, superior parietal and occipital association cortices. There is relative sparing of the primary visual cortices. Most intense cortical binding is seen in the primary sensorimotor and precentral cortices with lower hydrolysis rates in the anterior prefrontal areas. Interval changes include more severe posterior cortical losses and mid anterior-to-posterior prefrontal degeneration gradient (in both superior and orbitofrontal directions) and preservation of primary and secondary sensorimotor and peri-Sylvian cortices.

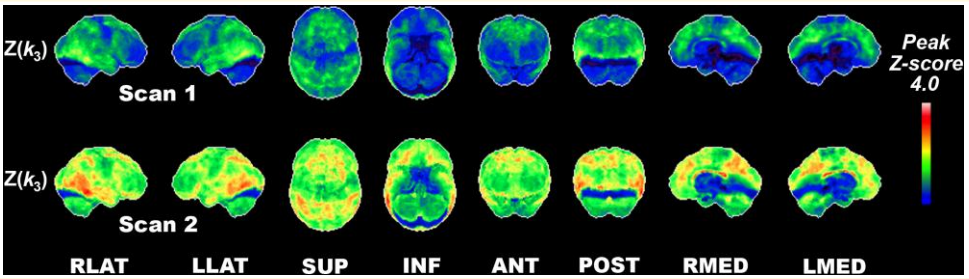


**Figure 2 Longitudinal regional cortical acetylcholinesterase hydrolysis reductions compared with normal controls.** Serial PMP $k_3$ *Z*-score maps over two-time points in Parkinson's disease compared with normal older control persons. Pronounced interval reductions (*Z*-scores $< -2$) were found in the occipital association cortices, posterolateral and inferior temporal regions, precuneus, posterior cingulum and to a lesser degree in the anterior mesofrontal regions were seen in the Parkinson's disease group.

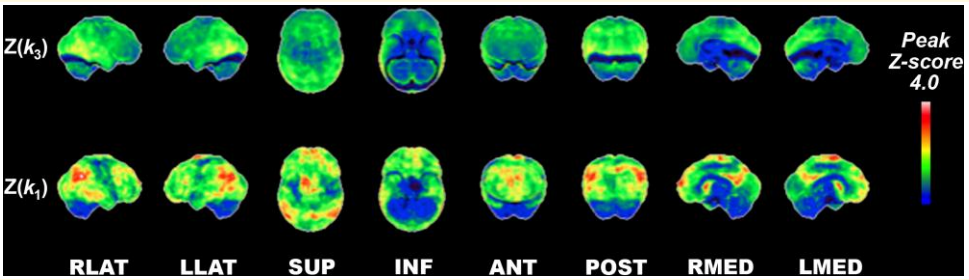


**Figure 3 Relative comparison of normative reductions of acetylcholinesterase hydrolysis rate versus proxy blood flow changes in the baseline Parkinson's disease group.** *Z*-scores based on comparison with normative data are presented. Relative comparison of $Z(k_3)$ to $Z(k_1)$ scores show striking topographic dissociation between vulnerability of cholinergic losses in Parkinson's disease compared with more prominent $k_1$ proxy blood flow reductions, in particular the superior and posterior parietal and anterior and inferior prefrontal cortices and reverse findings of relatively more prominent cholinergic reductions in the primary sensorimotor strip.

BA 25 (subgenual cortex) showed the greatest average per cent change in both $k_3$ [mean = −16.47%, standard deviation (SD) = 22.25%] and $k_1$ (mean = −5.1%, SD = 13.11%), along with greatest inter-subject variability. In terms of both average per cent change and per cent change variability of $k_3$, subgenual cortex was followed closely by BA 11 (orbitofrontal cortex; mean = −15.81%, SD = 14.19%), although the same does not hold for either average per cent change or per cent change variability in $k_1$ (mean = −2.59%, SD = 10.79%), both of which were lower. The orbitofrontal cortex shows the second highest $\%\Delta k_3$ over $\%\Delta k_1$ ratio value (6.12), indicating that the average per cent change in acetylcholinesterase $k_3$ of that region is greater relative to average per cent change in regional cerebral blood flow as compared with most other regions. The orbitofrontal cortex is only exceeded in that respect by BA 10, or the frontal pole, which shows the greatest ratio value (8.58), with an intermediate per cent change in $k_3$ (mean = −9.97%, SD = 9.09%) coupled with the lowest per cent change in $k_1$ (mean = −1.16%, SD = 10.63%) as compared with other regions included in our volume-of-interest-based BA analysis.

Examining the cortical surface plot of the $\%\Delta k_3$ over $\%\Delta k_1$ ratio (Fig. 4), a distinctive pattern is observed. The highest gradient of increasing ratio values occurs in the anterior cortices, from the subgenual cortex (3.23) to orbitofrontal cortex (6.12) to the frontal pole (8.59). More dorsal regions show a more modest increase in $\%\Delta k_3$ over $\%\Delta k_1$ ratio values from BA25 (3.23) to BA24 (3.46), or ventral anterior cingulate.

## Brodmann area volume-of-interest-based longitudinal mixed linear model analysis

Most of the regions selected based on the $\%\Delta k_3$ over $\%\Delta k_1$ ratio showed a significant effect of visit on $k_3$ while accounting for the $k_1$ regional cerebral blood flow proxy and individual differences in baseline $k_3$ (Table 2). The three regions for which visit had the strongest association with cholinergic nerve terminal integrity were subgenual cortex ($\beta = -0.94$, $P = 0.03$), orbitofrontal cortex ($\beta = -1.02$, $P = 0.01$) and frontal pole ($\beta = -0.88$, $P = 0.01$). The next strongest effect of the visit was observed in the ventral anterior cingulate ($\beta = -0.81$, $P = 0.01$). The remaining two significant effects of the visit were observed in BA 9 (dorsolateral/medial prefrontal cortex; $\beta = -0.81$, $P = 0.01$) and BA 6 (premotor cortex/supplementary motor area; $\beta = -0.72$, $P = 0.01$). The only region examined without a significant effect of the visit was BA 12 ($\beta = -0.39$, $P = 0.14$), which also showed the lowest per cent change in $k_3$ (mean = −5.52%, SD = 12.36%) and the second lowest per cent change

in $k_1$ (mean = −1.17%, SD = 13.09%) among the regions included in the cortical volume-of-interest analysis.

Of note is the fact that the adjusted $R^2$ for the non-significant BA12 model was 0.82, suggesting that $k_1$ proxy flow and baseline differences in $k_3$ robustly account for variability in acetylcholinesterase hydrolysis rates without taking visits into account. Most other regions showing a significant effect of the visit had a comparable adjusted $R^2$, ranging between 0.77 and 0.88, except for the subgenual cortex (*adj.* $R^2 = 0.39$) and the immediately anterior orbitofrontal cortex (*adj.* $R^2 = 0.65$). These were also the two regions with the strongest associations between acetylcholinesterase hydrolysis rates and visits. Lower adjusted $R^2$ values for those regions suggest that other factors may be at play when it comes to their change in $k_3$ hydrolysis rate.

## Subcortical volume-of-interest-based percentage difference between Visits 1 and 2

Among the four subcortical–limbic regions analysed (Table 3), the amygdala showed the greatest average per cent change and inter-individual variability in per cent change of $k_3$ (mean = −14.42%, SD = 18.76%) and the greatest average per cent change in $k_1$ proxy flow (mean = −7.41%, SD = 11.10%). The hippocampus shows the lowest average per cent change in $k_3$ (mean = −3.99%, SD = 14.72%) and the greatest variability in $k_1$ (mean = −5.56%, SD = 11.92%). It was the only region in either volume-of-interest-based analysis to show a $\%\Delta k_3$ over $\%\Delta k_1$ ratio <1.

## Subcortical volume-of-interest-based longitudinal mixed linear model analysis

Among the four exploratory models of regional $k_3$ (Table 4), amygdala ($\beta = -0.70$, $P = 0.02$) and insula ($\beta = -0.82$, $P = 0.01$) were the only ones to show a significant effect of visit. Adjusted $R^2$ for the four models ranged between 0.74 and 0.78, which means a comparable amount of variance in $k_3$ of subcortical regions is accounted for by their $k_1$ and individual differences in baseline $k_3$, with the visit making a significant contribution to the model's predictive capacity.

**Table 1 Mean and standard deviation of percentage change in PMP acetylcholinesterase $k_3$ and $k_1$ coefficients of cortical regions in volume-of-interests-based BA analysis, sorted in descending order based on $k_3/k_1$ ratio per cent changes**

| Region | $\%\Delta k_3/\%\Delta k_1$ | Mean % $\Delta k_3$ | SD % $\Delta k_3$ | Mean % $\Delta k_1$ | SD % $\Delta k_1$ |
|---|---|---|---|---|---|
| BA10 | 8.58 | −9.97 | 9.09 | −1.16 | 10.63 |
| BA11 | 6.12 | −15.81 | 14.19 | −2.59 | 10.79 |
| BA12 | 4.70 | −5.52 | 12.36 | −1.17 | 13.09 |
| BA24 | 3.46 | −9.68 | 8.96 | −2.80 | 10.18 |
| BA25 | 3.23 | −16.47 | 22.25 | −5.10 | 13.11 |
| BA9 | 2.92 | −8.46 | 9.39 | −2.89 | 11.24 |
| BA6 | 2.80 | −8.32 | 7.26 | −2.98 | 12.08 |

## Clinical predictors of longitudinal cholinergic system changes

None of our participants had auditory hallucinations or MCI and only one participant had visual hallucinations at follow-up. For that reason, MCI and hallucinations were excluded from this exploratory analysis. Eleven of 16 participants had RBD at baseline and the independent effect model was selected (*AIC* = 84.66, *adj.* $R^2 = 0.62$). The presence of RBD at baseline predicted significantly lower occipital–parietal $k_3$ ($\beta = -0.89$, $P = 0.027$) independent of visit ($\beta = -0.69$, $P = 0.003$). The interaction model was selected for both Stroop III (*AIC* = 83.17, *adj.* $R^2 = 0.68$) and Stroop IV (*AIC* = 82.76, *adj.* $R^2 = 0.70$). The marginal effect of the visit was negative and significant for both Stroop III ($\beta = -0.70$, $P = 0.008$) and Stroop IV ($\beta = -0.59$, $P = 0.022$), suggesting that occipital–parietal $k_3$ showed a significant decrease from baseline to the follow-up visit while holding Stroop performance at our sample's average. The interaction effect between visit and executive function trended in the expected positive direction for both Stroop III ($\beta = 0.39$, $P = 0.106$) and IV ($\beta = 0.49$, $P = 0.061$) tests, but neither effect reached significance. Descriptive statistics for examined clinical variables and all the relevant model coefficients are presented in Table 5.

# Discussion

Acetylcholinesterase activity has been long recognized as a marker for brain cholinergic synapses.[20, 47] Acetylcholinesterase is localized predominantly in cholinergic neuron perikarya, axons and synapses. Brain cholinergic systems are traditionally viewed as diffuse neuromodulator systems, but emerging evidence points to basal forebrain cholinergic projections exhibiting specific patterns of connectivity.[48] Basal forebrain neuron clusters give rise to extensive, multi-branch projections, with many neurons innervating a limited number of specific cortical fields[6, 26, 27] and an apparent organizing rule that clusters, at least partly, innervate interconnected cortical regions. Basal forebrain cholinergic system clusters may act independently with both relatively low temporal resolution (tonic) and fast (phasic) signalling.[28, 29, 49]

Our baseline findings indicate early vulnerability of the posterior, esp. lateral inferior temporal gyrus and angular gyrus cholinergic synapses, with slightly less affected medial occipital cortices and preservation of prefrontal and pericentral cortical areas when compared with normative *Z*-score mapping data of 61 older normal control individuals. Interval changes include more severe posterior cortical losses that follow a posterior-to-anterior progression of denervation as previously suggested by cross-sectional studies comparing Parkinson's disease dementia to Parkinson's disease.[18, 19] Contradicting a simple

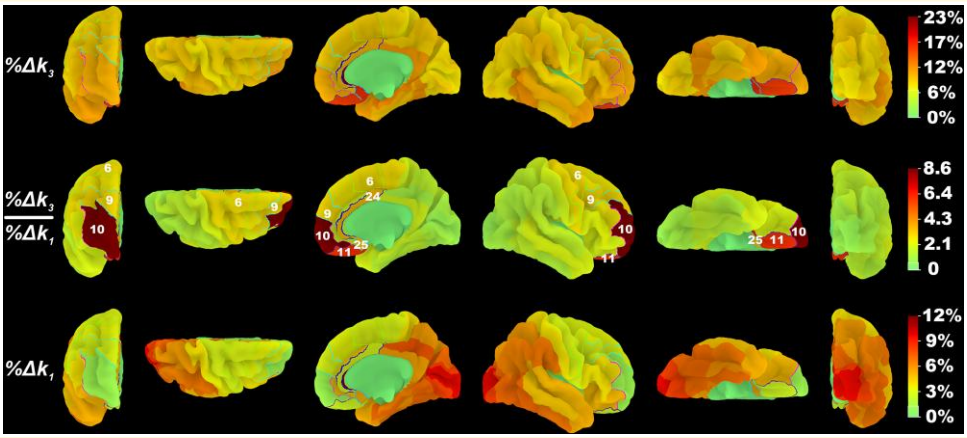


**Figure 4 Dissociation of $k_3$ acetylcholinesterase hydrolysis versus $k_1$ proxy flow changes in the anterior versus the posterior brain in the baseline Parkinson's disease group.** The percentage decrease in PMP $k_3$ and $k_1$ coefficients and the ratio of their percentage decrease from baseline visit to follow-up visit were mapped to BA volume-of-interests[42] and projected to a high-resolution cortical surface mesh. Regions for which the visit model fitted $k_3$ values significantly better than the confounding model are outlined and numbered based on their BA designation.

**Table 2 Summary table of BA volume-of-interest-based random intercept mixed linear models of regional $k_3$**

| Region | $\beta_{visit}$ | Std. error | CI 2.5% | CI 97.5% | $R^2$ | $R^2$ Adjusted | $\chi^2$ | *P*-Holm |
|---|---|---|---|---|---|---|---|---|
| BA10 | −0.88 | 0.20 | −1.26 | −0.49 | 0.81 | 0.78 | 12.92 | **0.01*** |
| BA11 | −1.02 | 0.24 | −1.48 | −0.55 | 0.69 | 0.65 | 12.46 | **0.01*** |
| BA12 | −0.39 | 0.19 | −0.76 | −0.03 | 0.84 | 0.82 | 3.97 | 0.14 |
| BA24 | −0.81 | 0.19 | −1.18 | −0.43 | 0.83 | 0.81 | 12.06 | **0.01*** |
| BA25 | −0.94 | 0.29 | −1.50 | −0.37 | 0.47 | 0.39 | 8.11 | **0.03*** |
| BA9 | −0.74 | 0.21 | −1.15 | −0.34 | 0.80 | 0.77 | 9.51 | **0.03*** |
| BA6 | −0.72 | 0.16 | −1.03 | −0.41 | 0.89 | 0.88 | 13.30 | **0.01*** |

$\beta$ coefficients are presented for the fixed effect of visit, with standard error of the coefficient and 95% confidence interval (CI) included. $\chi^2$ values obtained with likelihood ratio test were used to derive *P*-values for the visit models. Holm's method was used for family-wise error rate correction.[44]
*$P < 0.05$ family-wise error.

model of posterior-to-anterior progression of cortical cholinergic deficits, we also found evidence of a mid-frontal anterior-to-posterior cholinergic deficit progression (in both superior and orbitofrontal directions) with preservation of pericentral cortex cholinergic synapses. In concert with the posterior cortical brain posterior-to-anterior and anterior cortical brain anterior-to-posterior denervation gradients of interval progression we document, voxel-based percentage differences between Visits 1 and 2 demonstrated the greatest deficit progression in the subgenual cortex (up to 20% loss), followed by the mesial orbitofrontal cortex and gyrus rectus, followed by lateral occipital and lateral temporal cortices with lesser reductions in the anterior, inferior and mesial prefrontal cortex, posterior cingulum/precuneus and primary visual cortex.

The simultaneous presence of posterior-to-anterior gradient progressive denervation changes in the posterior brain and the anterior-to-posterior gradient in the anterior brain cannot be explained by a model of anatomically diffuse basal forebrain cholinergic projections succumbing to length-dependent stresses. Even within posterior cortices, we found evidence of relatively preserved primary occipital cortex tracer retention, immediately adjacent to cortical regions, lateral occipital, superior parietal, posterior and inferior lateral temporal cortices, with greater reductions in tracer retention. These results argue against the length-dependent vulnerability of basal forebrain cholinergic projections, as the primary visual cortex likely receives some of the longest basal forebrain cholinergic afferents.[20-22]

The pattern of posterior cortical cholinergic deficits points to significant cholinergic denervation of the so-called ventral visual stream.[50, 51] The ventral stream, passing from the primary visual cortex (V1) to the inferior parts of the temporal lobe, mediates the transformation of visual signals into mental constructs guiding memory, recognition and conscious perception. Our results are consistent with those of Luo *et al.*, who documented declines in temporo-occipital functional node connectivity, correlated with measures of visuoperceptual functions, in drug-naïve Parkinson's disease subjects. These observations imply that cholinergic changes in the inferior-occipital gyrus, fusiform gyrus and inferotemporal cortex may play an important role in the cognitive impairment syndrome of Parkinson's disease. This conclusion

is supported by a prior acetylcholinesterase PET study of MCI subjects: Haense *et al*. demonstrated that acetylcholinesterase reductions were most prominent in a lateral temporal cluster and correlated significantly with learning, executive and language comprehension functions. More speculatively, cholinergic denervation of the ventral stream might contribute to the common phenomenon of visual hallucinations in Parkinson's disease.[52] Our findings suggest an interplay of cholinergic deficits in the frontal and parietal regions that might distort the function of specific brain functional networks. We found that the interval progression of cortical cholinergic deficits includes key nodes of the default mode network, salience and (visual) attention networks. The default mode network is crucial for memory consolidation. The salience network triggers quick shifts from the default mode network's internal processing modes to external visual attentional processing via activation of the visual attention network. Loss of cholinergic synapses in these networks may contribute to Parkinson's disease cognitive deficits, including memory and attention deficits. Loss of salience functions, in conjunction with impaired ventral and dorsal visual stream functions, may degrade Parkinson's disease patients' ability to effectively detect and interpret visual cues, impairing safe ambulation in complex visual environments and contributing to characteristic illusions/hallucinations.

As previously reported, acetylcholinesterase $k_3$ was partially dissociated from $k_1$ regional cerebral blood flow proxy and regional glucose uptake.[18, 53] Relative comparison of the normalized regional $k_3$ to the $k_1$ *Z*-scores shows topographic dissociation between cholinergic synapse deficits and regional cerebral blood flow in Parkinson's disease. In the present study, the most prominent reductions in $k_1$ regional cerebral blood flow proxy were seen in superior and posterior parietal cortices. In contrast, we found evidence of reverse findings of relatively more prominent acetylcholinesterase $k_3$ deficits in the primary sensorimotor strip compared with corresponding minimal $k_1$ regional cerebral blood flow proxy changes. These results are consistent with a previous [$^{18}$F]-fluorodeoxyglucose glucose metabolic and [$^{11}$C]-PMP PET imaging study showing discordance between glucose metabolic and cholinergic synapse changes in Alzheimer's disease.[53] In that study, cholinergic synapse deficits involved the entire cerebral cortex, including the primary sensorimotor cortex. In contrast, glucose metabolic reductions primarily involved association cortices but sparing the primary sensorimotor cortices. We studied the relationship between cholinergic synapse deficit progression and regional cerebral blood flow more specifically by assessing interval changes based on $k_3/k_1$ ratio images ($k_3$ correction for regional cerebral blood flow proxy changes). This analysis showed disproportionate interval changes (up to 20%) in the ventral frontal, anterior cingulum and BA 6. In contrast, apparent $k_3$ interval reductions in posterior cortices, especially BA 17–19, were largely commensurate with $k_1$ changes. Regional cerebral blood flow, as assessed by $k_1$, correlates strongly with regional glucose uptake[54] and is conventionally interpreted as a measure of regional synaptic density. Cholinergic synapses are only a small fraction of cortical synapses, which are dominated by intracortical connections and thalamic afferents. The $k_3/k_1$ ratio is an index of changes in regional cholinergic synapse density relative to changes in total regional synaptic density. These observations suggest that the progression of cortical cholinergic deficits in Parkinson's disease may be mediated not only by general neurodegenerative processes affecting cortical synapses (*esp*. posterior cortex) but also by processes specific to basal forebrain cholinergic neurons (*esp*. anterior forebrain). Our cumulative results are consistent with the relative vulnerability of some clusters of basal forebrain cholinergic neurons. Potential clinical ramifications may include differential prediction of clinical responsiveness to cholinergic drugs or neurostimulation treatments with hypothesized prediction that clinical response to symptoms localizing in the posterior cortex or application of neurostimulation targeting the posterior brain may be less effective compared with similar applications of the anterior brain.

The dual syndrome hypothesis of cognitive impairment posits vulnerability of the posterior cortex due to cholinergic and other non-dopaminergic changes, whereas anterior changes

**Table 3 Mean and standard deviation of percentage changes in PMP acetylcholinesterase $k_3/k_1$ ratio coefficients of subcortical regions chosen for the volume-of-interest-based analysis not captured by the cortical 3D-SSP analysis, sorted in descending order based on the ratio of $k_3$ over $k_1$per cent change**

| Region | %$\Delta k_3$/% $\Delta k_1$ | Mean % $\Delta k_3$ | SD % $\Delta k_3$ | Mean % $\Delta k_1$ | SD % $\Delta k_1$ |
|---|---|---|---|---|---|
| Amygdala | 1.95 | −14.42 | 18.76 | −7.41 | 11.10 |
| Insula | 1.38 | −9.18 | 11.22 | −6.63 | 11.78 |
| Thalamus | 1.37 | −6.09 | 11.29 | −4.46 | 9.07 |
| Hippocampus | 0.71 | −3.99 | 14.72 | −5.65 | 11.92 |

**Table 4 Summary table of subcortical volume-of-interest-based random intercept mixed linear models of regional $k_3$**

| Region | $\beta_{visit}$ | Std. error | CI 2.5% | CI 97.5% | $R^2$ | $R^2$ adjusted | $\chi^2$ | *P* |
|---|---|---|---|---|---|---|---|---|
| Amygdala | −0.70 | 0.23 | −1.15 | −0.26 | 0.80 | 0.77 | 7.51 | **0.02** |
| Insula | −0.82 | 0.22 | −1.26 | −0.38 | 0.80 | 0.77 | 9.76 | **0.01** |
| Thalamus | −0.29 | 0.21 | −0.71 | 0.13 | 0.81 | 0.78 | 1.67 | 0.43 |
| Hippocampus | −0.17 | 0.23 | −0.61 | 0.28 | 0.77 | 0.74 | 0.53 | 0.77 |

$\beta$ coefficients are presented for the fixed effect of visit, with standard error of the coefficient and 95% confidence interval (CI) included. $\chi^2$ values obtained with likelihood ratio test were used to derive *P*-values for the visit models. No family-wise error rate correction was employed due to the exploratory nature of this *post hoc* analysis.

**Table 5 Summary table of *post hoc* clinical regressor effect of occipital–parietal $k_3$ analysis**

| Regressor | Baseline | Follow-up | $\beta_{visit}$ | $\beta_{clinical}$ | $\beta_{visit*clinical}$ |
|---|---|---|---|---|---|
| DKEFS Stroop III | 122.20 ± 29.92 | 140.69 ± 39.79 | **−0.70** | −0.12 | 0.39 |
| DKEFS Stroop IV | 137.28 ± 29.77 | 159.33 ± 45.59 | **−0.59** | −0.38 | 0.49 |
| RBD | 11/16 | | **−0.69** | **−0.89** | |

$\beta$ coefficients are presented for selected AIC minimizing model. If the independent effect model was selected, $\beta$ coefficients for independent effect of visit ($\beta_{visit}$) and clinical regressor ($\beta_{clinical}$) are presented. If the interaction model was selected, $\beta$ coefficients for the marginal effect of visit ($\beta_{visit}$), marginal effect of clinical regressor ($\beta_{clinical}$) and visit by clinical regressor interaction term ($\beta_{visit*clinical}$) are presented. Statistically significant model effects ($P < 0.05$) are bolded. Descriptive statistics for the clinical regressors are presented for baseline and follow-up visit as mean ± SD for Stroop measures and as ratio of participants for RBD. DKEFS = Delis–Kaplan Executive Function System; RBD = rapid eye movement sleep behaviour disorder.

are attributed to frontostriatal dopaminergic system dysfunctions.[17, 55] Although our observation of more prominent cholinergic losses in the posterior brain provides partial support for this model of cognitive impairment in Parkinson's disease, findings of a reverse (i.e. posterior-to-anterior) progressive cholinergic denervation gradient in the prefrontal brain imply that this model is too simplistic and ignores a potential contribution of frontal cholinergic deficits to progressive cognitive decline in Parkinson's disease.[56]

Our supplemental analysis of subcortical–limbic structures—not captured by the cortical 3D-SSP analysis—is consistent with the relatively selective involvement of different cholinergic projection system components. The insula and amygdala, which receive cholinergic innervation from the posterior basal forebrain, also demonstrated interval cholinergic synapse losses, but not the hippocampus, which receives cholinergic afferents from the more anterior basal forebrain, or the thalamus, which receives cholinergic innervation from mesopontine neurons.

Although our *post hoc* analysis of RBD and Stroop measures of executive function in relation to occipital–parietal $k_3$ failed to yield a model with a significant visit by clinical regressor interaction term, the interaction models demonstrated the lowest AIC for Stroop measures of executive function as compared with random intercept, visit-only and independent effect models. Furthermore, the interaction term in the Stroop regressor models trended in the expected positive direction, which suggests that greater time to complete tasks that require top-down inhibitory control of attention and task switching may be associated with a stronger effect of visit on longitudinal cholinergic losses in the occipital–parietal cortices.

A limitation of the PMP radioligand is that it does not allow accurate assessment of the high acetylcholinesterase activity levels in the striatum and cerebellum. Longitudinal changes in these subcortical areas could not be assessed in this study. Another potential limitation is the possibility that acetylcholinesterase expression or activity is regulated, potentially degrading the relationship between $k_3$ and cholinergic synaptic density.[57] Our $k_3/k_1$ ratio analysis also presupposes that there is no independent effect of basal forebrain cholinergic afferents on the regulation of regional cerebral blood flow, which may be an over-simplification.[58, 59] Our study was based on a convenience predominant male study sample, limiting generalization for the female gender. Lastly, due to the relatively small sample size, the possibility of Type II statistical error on non-significant and marginally significant findings in this study cannot be ruled out.

We conclude that our findings only partially support a posterior-to-anterior progression of cortical cholinergic deficits in Parkinson's disease. We found a reverse frontal lobe pattern of more intrinsic progressive cholinergic deficits. All in total, our results are consistent with differential anatomic and temporal degeneration of clusters of basal forebrain cholinergic projections. Our observations suggest that cortical cholinergic deficits in Parkinson's disease are mediated by processes specific to cholinergic basal forebrain neurons and a general loss of cortical synapses.

## Acknowledgements

The authors thank Christine Minderovic, Virginia Rogers, the PET technologists, cyclotron operators, and chemists, for their assistance. This work was supported by the Department of Veterans Affairs, the Michael J. Fox Foundation, the Parkinson's Foundation, and NIH grants P01 NS015655, RO1 NS070856, P50 NS091856 & P50 NS123067.

## Funding

The authors have received research funding from the National Institutes of Health (P01 NS015655, RO1 NS070856, R21 AG069387; R01 AG073100; P50 NS123067), Department of Veterans Affairs (I01 RX003397), Parkinson's Foundation, the Farmer Family Foundation Parkinson's Research Initiative, and the Michael J. Fox Foundation.

## Competing interests

The authors declare no conflict of interest relevant to this work.

## Data availability

Data are available to qualified investigators upon reasonable request.

# References


1. Cumming P, Borghammer P. Molecular imaging and the neuropathologies of Parkinson's disease. *Curr Top Behav Neurosci*. 2012;11:117-148.
2. Arendt T, Bigl V, Arendt A, Tennstedt A. Loss of neurons in the nucleus basalis of meynert in Alzheimer's disease, paralysis agitans and Korsakoff's disease. *Acta Neuropathol (Berl)*. 1983;61:101-108.
3. Bohnen NI, Yarnall AJ, Weil RS, *et al*. Cholinergic system changes in Parkinson's disease: Emerging therapeutic approaches. *Lancet Neurol*. 2022;21(4):381-392.
4. Albin RL, van der Zee S, van Laar T, *et al*. Cholinergic systems, attentional-motor integration, and cognitive control in Parkinson's disease. *Prog Brain Res*. 2022;269(1):345-371.
5. Schmitz TW, Zaborszky L. Spatial topography of the basal forebrain cholinergic projections: Organization and vulnerability to degeneration. *Handb Clin Neurol*. 2021;179:159-173.
6. Ballinger EC, Ananth M, Talmage DA, Role LW. Basal forebrain cholinergic circuits and signaling in cognition and cognitive decline. *Neuron*. 2016;91(6):1199-1218.
7. Heckers S, Geula C, Mesulam M. Cholinergic innervation of the human thalamus: Dual origin and differential nuclear distribution. *J Comp Neurol*. 1992;325:68-82.
8. Mena-Segovia J, Bolam JP. Rethinking the pedunculopontine nucleus: From cellular organization to function. *Neuron*. 2017; 94(1):7-18.
9. Gut NK, Mena-Segovia J. Dichotomy between motor and cognitive functions of midbrain cholinergic neurons. *Neurobiol Dis*. 2019; 128:59-66.
10. Agid Y, Cervera P, Hirsch E, *et al*. Biochemistry of Parkinson's disease 28 years later: A critical review. *Mov Disord*. 1989;4(Suppl 1): S126-S144.
11. Candy JM, Perry EK, Perry RH, Court JA, Oakley AE, Edwardson JA. The current status of the cortical cholinergic system in Alzheimer's disease and Parkinson's disease. *Prog Brain Res*. 1986;70:105-132.
12. Liu AK, Chang RC, Pearce RK, Gentleman SM. Nucleus basalis of meynert revisited: Anatomy, history and differential involvement in Alzheimer's and Parkinson's disease. *Acta Neuropathol*. 2015; 129(4):527-540.
13. Kuhl DE, Minoshima S, Fessler JA, *et al*. In vivo mapping of cholinergic terminals in Normal aging, Alzheimer's disease, and Parkinson's disease. *Ann Neurol*. 1996;40(3):399-410.
14. Shinotoh H, Namba H, Yamaguchi M, *et al*. Positron emission tomographic measurement of acetylcholinesterase activity reveals differential loss of ascending cholinergic systems in Parkinson's disease and progressive supranuclear palsy. *Ann Neurol*. 1999;46:62-69.
15. Bohnen NI, Kaufer DI, Ivanco LS, *et al*. Cortical cholinergic function is more severely affected in parkinsonian dementia than in Alzheimer disease: An in vivo positron emission tomographic study. *Arch Neurol*. 2003;60(12):1745-1748.
16. Hilker R, Thomas AV, Klein JC, *et al*. Dementia in Parkinson disease: Functional imaging of cholinergic and dopaminergic pathways. *Neurology*. 2005;65(11):1716-1722.
17. Kehagia AA, Barker RA, Robbins TW. Cognitive impairment in Parkinson's disease: The dual syndrome hypothesis. *Neurodegener Dis*. 2012;11(2):79-92.
18. Kuhl DE, Koeppe RA, Minoshima S, *et al*. In vivo mapping of cerebral acetylcholinesterase activity in aging and Alzheimer's disease. *Neurology*. 1999;52(4):691-699.
19. Klein JC, Eggers C, Kalbe E, *et al*. Neurotransmitter changes in dementia with Lewy bodies and Parkinson disease dementia in vivo. *Neurology*. 2010;74(11):885-892.
20. Selden NR, Gitelman DR, Salamon-Murayama N, Parrish TB, Mesulam MM. Trajectories of cholinergic pathways within the cerebral hemispheres of the human brain. *Brain*. 1998;121(Pt 12): 2249-2257.
21. Kitt CA, Mitchell SJ, DeLong MR, Wainer BH, Price DL. Fiber pathways of basal forebrain cholinergic neurons in monkeys. *Brain Res*. 1987;406(1–2):192-206.
22. Bigl V, Woolf NJ, Butcher LL. Cholinergic projections from the basal forebrain to frontal, parietal, temporal, occipital, and cingulate cortices: A combined fluorescent tracer and acetylcholinesterase analysis. *Brain Res Bull*. 1982;8(6):727-749.
23. Wu H, Williams J, Nathans J. Complete morphologies of basal forebrain cholinergic neurons in the mouse. *Elife*. 2014;3:e02444.
24. Ovsepian SV, O'Leary VB, Hoschl C, Zaborszky L. Integrated phylogeny of the human brain and pathobiology of Alzheimer's disease: A unifying hypothesis. *Neurosci Lett*. 2021;755:135895.
25. Shekari A, Fahnestock M. Retrograde axonal transport of neurotrophins in basal forebrain cholinergic neurons. *Methods Mol Biol*. 2022;2431:249-270.
26. Gielow MR, Zaborszky L. The input-output relationship of the cholinergic basal forebrain. *Cell Rep*. 2017;18(7):1817-1830.
27. Zaborszky L, Csordas A, Mosca K, *et al*. Neurons in the basal forebrain project to the cortex in a complex topographic organization that reflects corticocortical connectivity patterns: An experimental study based on retrograde tracing and 3D reconstruction. *Cereb Cortex*. 2015;25(1):118-137.
28. Sarter M, Lustig C. Cholinergic double duty: Cue detection and attentional control. *Curr Opin Psychol*. 2019;29:102-107.
29. Gombkoto P, Gielow M, Varsanyi P, Chavez C, Zaborszky L. Contribution of the basal forebrain to corticocortical network interactions. *Brain Struct Funct*. 2021;226(6):1803-1821.
30. Shinotoh H, Namba H, Fukushi K, *et al*. Progressive loss of cortical acetylcholinesterase activity in association with cognitive decline in Alzheimer's disease: A positron emission tomography study. *Ann Neurol*. 2000;48(2):194-200.
31. Hughes AJ, Daniel SE, Kilford L, Lees AJ. Accuracy of clinical diagnosis of idiopathic Parkinson's disease: A clinico-pathological study of 100 cases. *J Neurol Neurosurg Psychiatry*. 1992;55(3):181-184.
32. Bohnen NI, Kanel P, Muller M. Molecular imaging of the cholinergic system in Parkinson's disease. *Int Rev Neurobiol*. 2018;141: 211-250.
33. Thompson CJ, Kecani S, Boelen S. Evaluation of a neck-shield for use during neurological studies with a whole-body PET scanner. *IEEE Trans Nucl Sci*. 2001;48:1512-1517.
34. Snyder SE, Tluczek L, Jewett DM, Nguyen TB, Kuhl DE, Kilbourn MR. Synthesis of 1-[$^{11}$C]methylpiperidin-4-yl propionate ([$^{11}$C] PMP) for in vivo measurements of acetylcholinesterase activity. *Nucl Med Biol*. 1998;25:751-754.
35. Bohnen NI, Muller MLTM, Kotagal V, *et al*. Olfactory dysfunction, central cholinergic integrity and cognitive impairment in Parkinson disease. *Brain*. 2010;133:1747-1754.
36. Minoshima S, Koeppe RA, Fessler JA, *et al*. Integrated and automated data analysis method for neuronal activation studying using O15 water PET. In: Uemura K Lassen NA Jones T and Kanno I, eds. *Quantification of brain function to tracer kinetics and image analysis in brain PET*. Excerpta Medica; 1993:409-418.
37. Nagatsuka S, Fukushi K, Shinotoh H, *et al*. Kinetic analysis of [($^{11}$)C]MP4A using a high-radioactivity brain region that represents an integrated input function for measurement of cerebral acetylcholinesterase activity without arterial blood sampling. *J Cereb Blood Flow Metab*. 2001;21(11):1354-1366.
38. Koeppe RA, Frey KA, Snyder SE, Meyer P, Kilbourn MR, Kuhl DE. Kinetic modeling of N-[$^{11}$C]methylpiperidin-4-yl propionate: Alternatives for analysis of an irreversible positron emission tomography tracer for measurement of acetylcholinesterase activity in human brain. *J Cereb Blood Flow Metab*. 1999;19:1150-1163.
39. Talairach J, Tournoux P. *Co-planar stereotaxic atlas of the human brain*. Thieme; 1988.
40. Minoshima S, Koeppe RA, Frey KA, Kuhl DE. Anatomic standardization: Linear scaling and nonlinear warping of functional brain images. *J Nucl Med*. 1994;35:1528-1537.

41. Minoshima S, Frey KA, Koeppe RA, Foster NL, Kuhl DE. A diagnostic approach in Alzheimer's disease using three-dimensional stereotactic surface projections of fluorine-18-FDG PET. *J Nucl Med*. 1995;36:1238-1248.
42. Pijnenburg R, Scholtens LH, Ardesch DJ, de Lange SC, Wei Y, van den Heuvel MP. Myelo- and cytoarchitectonic microstructural and functional human cortical atlases reconstructed in common MRI space. *Neuroimage*. 2021;239:118274.
43. Abraham A, Pedregosa F, Eickenberg M, *et al*. Machine learning for neuroimaging with scikit-learn. *Front Neuroinform*. 2014;8:14.
44. Holm S. A simple sequentially rejective multiple test procedure. *Scan J Statistics*. 1979;6(2):65-70.
45. Seabold S, Perktold J. *Statsmodels: Econometric and statistical modeling with python*. In: *Proceedings of the 9th Python in Science Conference*. SCIPY. 2010:92-96.
46. Bohnen N, Jolles J, Twijnstra A. Modification of the stroop color word test improves differentiation between patients with mild head injury and matched controls. *Clinical Neuropsychologist*. 1992;6(2):178-184.
47. Shute CC, Lewis PR. Electron microscopy of cholinergic terminals and acetylcholinesterase-containing neurones in the hippocampal formation of the rat. *Zellforsch Mikrosk Anat*. 1966;69:334-343.
48. Záborszky L, Gombkoto P, Varsanyi P, *et al*. Specific basal forebrain-cortical cholinergic circuits coordinate cognitive operations. *J Neurosci*. 2018;38(44):9446-9458.
49. Sarter M, Lustig C. Forebrain cholinergic signaling: Wired and phasic, not tonic, and causing behavior. *J Neurosci*. 2020;40(4):712-719.
50. Kravitz DJ, Saleem KS, Baker CI, Ungerleider LG, Mishkin M. The ventral visual pathway: An expanded neural framework for the processing of object quality. *Trends Cogn Sci*. 2013;17(1):26-49.
51. Milner AD. How do the two visual streams interact with each other? *Exp Brain Res*. 2017;235(5):1297-1308.
52. Boes AD, Prasad S, Liu H, *et al*. Network localization of neurological symptoms from focal brain lesions. *Brain*. 2015;138(Pt 10):3061-3075.
53. Minoshima S, Cross DJ, Foster NL, Henry TR, Kuhl DE. Discordance between traditional pathologic and energy metabolic changes in very early Alzheimer's disease. Pathophysiological implications. *Ann N Y Acad Sci*. 1999;893:350-352.
54. Koeppe RA, Gilman S, Joshi A, *et al*. $^{11}$C-DTBZ and $^{18}$F-FDG PET measures in differentiating dementias. *J Nucl Med*. 2005;46(6):936-944.
55. Williams-Gray CH, Foltynie T, Brayne CE, Robbins TW, Barker RA. Evolution of cognitive dysfunction in an incident Parkinson's disease cohort. *Brain*. 2007;130(Pt 7):1787-1798.
56. van der Zee S, Kanel P, Gerritsen MJJ, *et al*. Altered cholinergic innervation in De Novo Parkinson's disease with and without cognitive impairment. *Mov Disord*. 2022;37(4):713-723.
57. DeKosky ST, Ikonomovic MD, Styren SD, *et al*. Upregulation of choline acetyltransferase activity in hippocampus and frontal cortex of elderly subjects with mild cognitive impairment. *Ann Neurol*. 2002;51(2):145-155.
58. Vaucher E, Hamel E. Cholinergic basal forebrain neurons project to cortical microvessels in the rat: Electron microscopic study with anterogradely transported Phaseolus vulgaris leucoagglutinin and choline acetyltransferase immunocytochemistry. *J Neurosci*. 1995;15(11):7427-7441.
59. Vaucher E, Linville D, Hamel E. Cholinergic basal forebrain projections to nitric oxide synthase-containing neurons in the rat cerebral cortex. *Neuroscience*. 1997;79(3):827-836.